MuCell® technology for injection molding: A processing method for polyether-urethane scaffolds

S. LEICHER, J. WILL, H. HAUGEN, E. WINTERMANTEL
Central Institute for Medical Engineering ZIMT,Technische Universität München, Boltzmannstrasse 11, D-85748, Garching bei München, Germany

MuCell® injection molding technology which takes supercritical carbon dioxide as blowing agent was used as processing method to generate porous samples made of thermoplastic polyether-urethane. The influence of processing parameters on the morphology of the porous structures was examined by mercury intrusion porometry and image analysis. An increase in injection speed and content of CO_2 in the polymer melt decreased pore sizes whereas an increase in the percentage of weight reduction increased pore sizes. Polyether-urethane samples with porosities of 70% and pore sizes from 184 to 1102 μm were observed. Interconnective pore sizes ranged from 40 to 275 μm.

1. Introduction

Present approaches for fabricating porous polymer structures for biomedical applications include particulate leaching methods [1–3], phase separation [4], emulsion freeze-drying [5], and combinations of these. The named techniques use organic solvents which may be left in the scaffold and might cause inflammatory reactions [6]. Newer approaches like carbon dioxide expansion avoid these solvents [6]. Nevertheless, all afore mentioned methods are limited in number and size of the samples due to laboratory handling. No ideal scaffold processing technique suited for industrial production of porous scaffolds is yet known.

Haugen [7, 8] developed a polymer foaming method for injection molding which uses water as non toxic blowing agent combined with a salt leaching technique. Although this method is simple and is able to produce scaffolds with high porosities and pore sizes in the desired range, the major drawback of the process is the time-consuming preparation of the polymer and the necessary leaching step. Also, the hydrolysis of the chosen thermoplastic polyether-urethane at high temperatures in the presence of water [9] is a disadvantage.

In this study, the MuCell® injection molding technology which uses benign gas as blowing agent was observed concerning its ability to work as a large scale scaffold processing method for biomedical engineering. The parameters of the process and their influence on pore morphology were examined. As there are a large number of dependent process parameters, it was necessary to focus on key parameters. Fixed process parameters were the cooling time, plasticize pressure and microcellular process pressure (MPP), temperature of the heating bands and plasticizing rotation whereas the changeable parameters were CO_2 weight gain, percentage of weight reduction, injection speed, and temperature of the mold. The choice of the changeable parameters was done based on the knowledge given by nucleation theory and literature data [7, 10]. Rodeheaver and Colton [11] found that an increased foaming temperature is an important factor to achieve a high content of open pores. Therefore, the highest possible temperature for the chosen material was set on the heating bands. Samples were produced by varying one parameter while the others were held constant. Thus, the influence of each processing parameter on the pore morphology could easily be observed. After processing, the samples were subsequently analyzed using mercury intrusion porometry, optical analysis and mechanical tests.

2. Materials and methods

2.1. Polymer processing

Thermoplastic polyether-urethane (TPU) (Texin® 985, Bayer Plastics Division, Pittsburgh, PA, USA) was chosen to process the samples. An injection molding machine (KM 125 C2, Krauss Maffei GmbH, Munich, Germany) with a mold temperature controlling device (90 S, Regloplas GmbH, Munich, Germany) was used for the mass production of the porous samples. The injection molding machine was equipped with a MuCell® package by the manufacturer. This package contains a special plasticizing unit (Sp220 MuCell® plasticizing unit with a screw diameter of 25.0 mm and an adaptor for Sp520 plasticize unit, Krauss Maffei GmbH, Munich, Germany) with one supercritical fluid (SCF) injection valve (25 mm series II injector, Trexel Inc., Woburn, MA, USA). It also includes a SCF metering system that consists of a SCF

0022-2461 © *2005 Springer Science + Business Media, Inc.*
DOI: 10.1007/s10853-005-0853-y

TABLE I Variable and fixed parameters while processing

Variable parameters	Examined range
CO_2 weight gain	1.6–6.3 wt%
Percentage of weight reduction (compared to bulk part)	25–59%
Injection speed	30–150 mm/s
Fixed parameters	**Value**
Cooling time	65 s
Injection pressure	1500 bar
Plasticize pressure	200 bar
MPP	200 bar
Dwell pressure	200 bar
Beginning dwell pressure	5 mm
Duration of dwell pressure	0.5 s
Clamp tonnage	200 kN
Temperature of the heating bands	180–210°C
Temperature of the mold	40°C
Plasticizing rotation	60 min^{-1}

delivery system (TE-3 series II, Trexel Inc., Woburn, MA, USA) and piping as well as instrumentation. The used mold was capable to produce six toroid-shaped samples with an outer diameter of 31 mm and a thickness of 10 mm at one shot. Table I gives an overview over the fixed parameters and shows the analyzed range of the variable parameters that were used during the experiments.

2.2. Porometry

Mercury intrusion porometry (AutoPore IV 9500, Micromeritics Instrument Corporation, Norcross, GA, USA) was applied to determine pore size distribution and porosity of the samples. The porous polymer samples were placed in a solid penetrometer with 5 ml bulb volume (Solid 5 cc, Pen Stem.38 cc, Micromeritics Instrument Corporation, Norcross, GA, USA). The intrusion chamber was then filled with mercury and the samples were penetrated with mercury until a maximum pressure of 110 MPa, where the total intrusion volume reached a plateau. A curve resulting from a measurement consists of 120 measure points, the lines in Fig. 1 are drawn to guide the eyes only. The peak of a curve gives the mean pore size diameter. Mercury intrusion measurements were done at samples produced with an injection speed of 30 and 150 mm/s, a percentage of weight reduction of 27 and 59%, and a content of carbon dioxide of 1.6 respectively 6.3%. The processing conditions that were used to produce the samples for mercury intrusion porometry are shown in Table II.

TABLE II Processing conditions to produce the samples

	CO_2 content	Percentage of weight reduction	Injection speed
Varying the injection speed	1.8%	25%	–
Varying the percentage of weight reduction	2.5%	–	150 mm/s
Varying the content of CO_2	–	57%	150 mm/s
Overall porosity	6.3%	59%	150 mm/s

2.3. Image analysis

Scanning electron microscope (SEM) (S-3500 N, Hitachi Science Systems, Tokyo, Japan) was used for observation of the internal pore morphology. The porous samples were sliced with a scalpel and then coated with gold by using a sputter-coater (SCD 005, BAL-TEC AG, Balzers, Lichtenstein). The morphology of the pores and the connections was evaluated by using image-processing analysis (Cellenger 4.0, Definiens AG, Munich, Germany) based on SEM micrographs. The rule sets were created especially for this application and are explained in the following. The area of an image object is the number of pixels forming it.

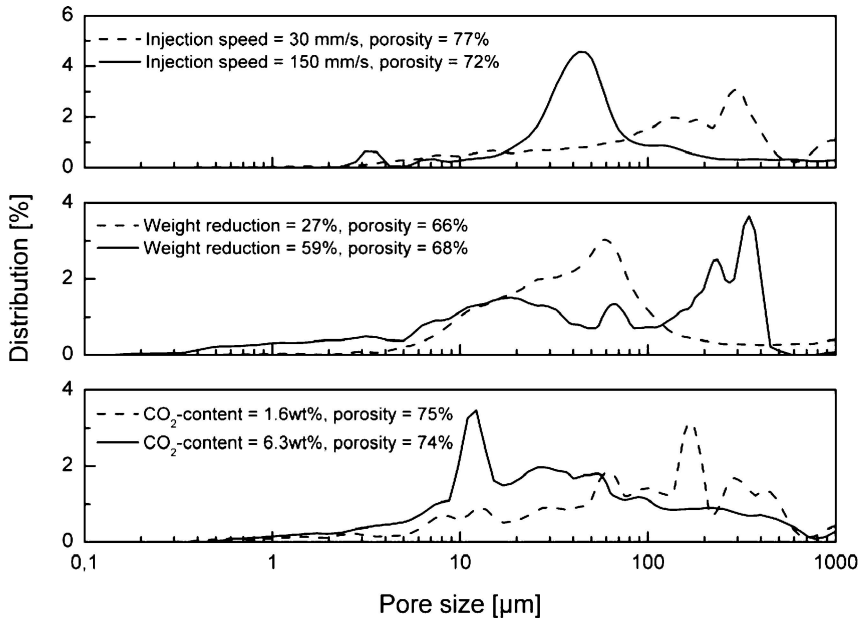

Figure 1 Pore size distribution as a function of the injection speed (*top*), the percentage of weight reduction and the content of carbon dioxide (*bottom*).

TABLE III Parameters for the quasi-static tensile-test

Parameters	Value
Ambient medium	Air, room temperature
Initial load	5 N
Initial load speed	50 mm/min
Test speed	500 mm/min
Load cell	2.5 kN

Derived from the object area is the pore diameter which gives the diameter of a round pore with the same area. The average diameter of all pores that can be found in one image is the mean pore diameter. In the following this value is referred to as median pore diameter and describes the size of the interconnections of adjacent voids. Due to the fact that the pores shown in the micrographs are two-dimensional projections of three-dimensional objects, their maximum diameter may not be represented in the image. To consider this, a factor of 0.616 was used to determine the maximum spherical diameter, called corrected median pore diameter, from the measured median pore diameter. Image analysis was done at samples produced with an injection speed of 30 to 150 mm/s in increments of 30 mm/s, a percentage of weight reduction of 27 and 59%, and a content of carbon dioxide of 1.6 respectively 6.3 wt%. Table II gives the processing conditions that were used to produce the samples for mercury intrusion porometry and image analysis.

2.4. Mechanical analysis

Ring shaped samples went through a quasi-static tensile-test with a material testing machine (TC-FR 2.5TS.D09, Zwick GmbH & Co., Ulm, Germany) under conditions defined by DIN 53504. Table III lists the chosen experimental parameters. The tested samples were processed with an injection speed of 150 mm/s, a gas content of 2.15 wt% (±0.35%) and a percentage of weight reduction of 25 respectively 59%.

3. Results

3.1. Porometry

Fig. 1 shows the influence of the injection speed, the percentage of weight reduction, and the content of carbon dioxide on pore morphology, measured by mercury intrusion porometry. At a speed of 30 mm/s the mean pore size diameter (top section of Fig. 1) was at 300 μm with a porosity of 77%. An increase of the injection speed to 150 mm/s shifted the mean pore size to 45 μm with a porosity of 72%. The pore size distribution of the samples processed with 150 mm/s was narrower than the distribution obtained at the injection speed of 30 mm/s. The mean pore size diameter at 59% weight reduction (middle section of Fig. 1) was at 345 μm with a porosity of 68%. At a percentage of weight reduction of 27% the mean pore size was at 60 μm with a porosity of 66%. At 59% weight reduction a very broad pore distribution with several peaks of mercury intrusion was visible, whereas at the lower percentage of weight reduction the pore size distribution was narrower. The most common pore size for samples processed with 1.6 wt% carbon dioxide (bottom section of Fig. 1) was 165 μm with a porosity of 74%. A gas content increase to 6.3 wt% shifted the mean pore size diameter to 12 μm with a porosity of 75%. The pore size distribution of both curves was of nearly similar shape. Table IV displays the average porosities and standard deviations of the tested samples. The porosity of one molded part was 70.4 ± 3.8%. Samples taken from six different toroids of one shot showed an average porosity of 69.6 ± 2.9%. The porosity of samples taken from a series of molded parts was 69.5 ± 2.7%. This leaded to an overall porosity of 69.9 ± 3.2%.

TABLE IV Average porosity and Standard deviation. A molded part consists of six toroid-shaped samples, the sprue and the runner system

Tested samples	Average porosity
One toroid ($n = 7$)	70.4 ± 3.8%
One moulded part ($n = 6$)	69.6 ± 2.9%
Series of moulded parts ($n = 6$)	69.5 ± 2.7%
Overall porosity ($n = 19$)	69.9 ± 3.2%

3.2. Image analysis

Typical SEM micrographs of samples processed with different injection speeds can be seen in Fig. 2. The pictures display that pore size decreased with an increase in injection speed from 30 (left) to 150 mm/s. Further on an orientation of the pores depending on the flow path of the polymer melt was apparent. The morphology of the pores at different percentages of

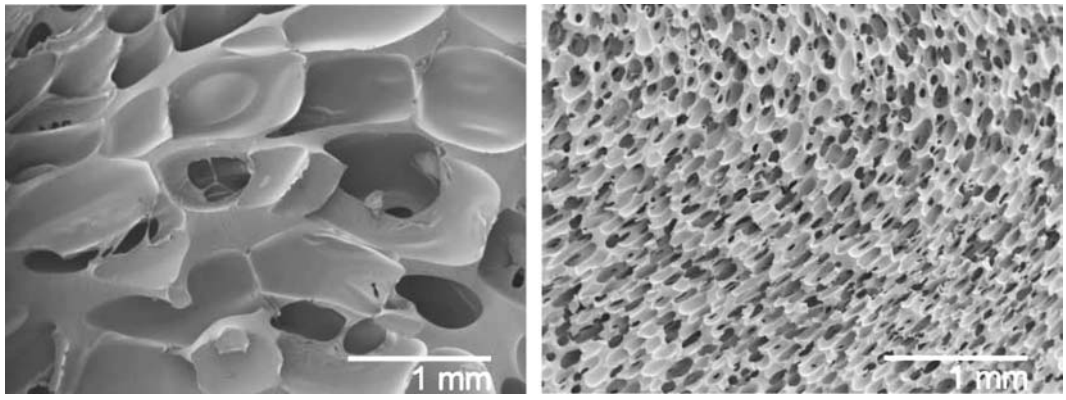

Figure 2 Pore morphology at injection speeds of 30 (*left*) respectively 150 mm/s.

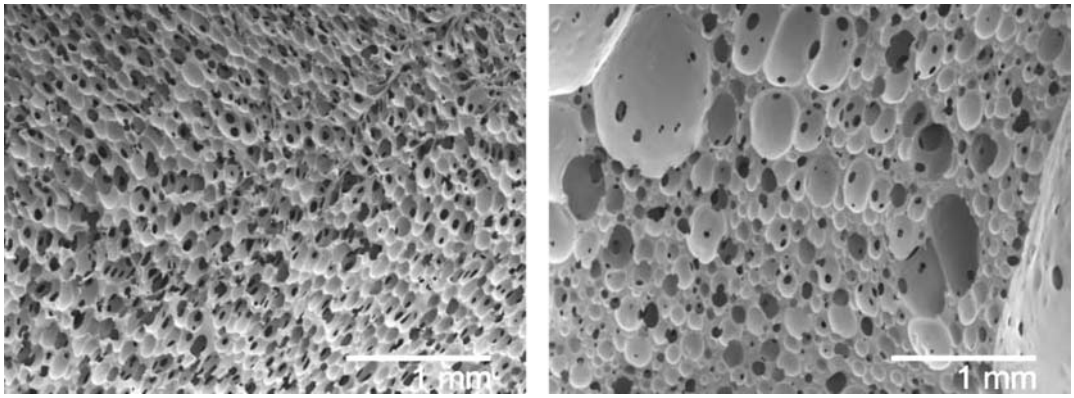

Figure 3 Pore morphology at 27 (*left*) and 59% of weight reduction.

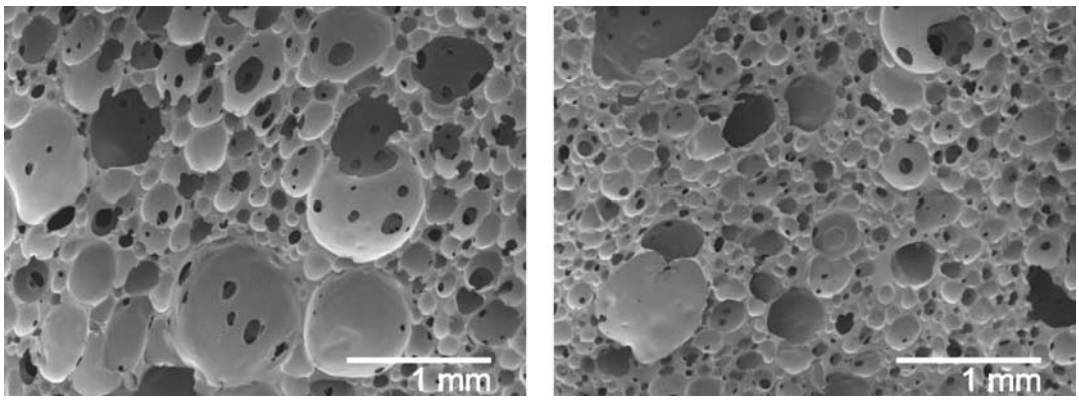

Figure 4 Pore morphology at 1.6 (*left*) and 6.3 wt% of gas content.

TABLE V Diameters of the connections between neighboring pores in dependence on the variable parameters

Parameter	Value	Median pore diameter
Injection speed	30 mm/s	275 ± 89 μm
	150 mm/s	53 ± 27 μm
Percentage of weight reduction	27%	40 ± 15 μm
	59%	59 ± 25 μm
Content of CO_2	1.6 wt%	85 ± 45 μm
	6.3 wt%	50 ± 19 μm

weight reduction is shown in Fig. 3. The most obvious difference between the pictures was that at 27% weight reduction (left) the pores had a uniform structure. On the other hand at higher weight reduction (59%) the pores differ much in size. Samples processed with different gas contents are visible in Fig. 4. The structure with the gas content of 6.3 wt%, shown on the right side, contained more small pores and also seemed to be less interconnective.

Fig. 5 and Table V present the computational analysis of the SEM micrographs. Fig. 5 describes the influence of the injection speed, the percentage of weight reduction, and the content of carbon dioxide on the corrected median pore diameter. An increase in injection speed decreased pore sizes. At an injection speed of 150 mm/s the most uniform structure with median pore sizes of 284 ± 29 μm could be found. An injection speed of 30 mm/s generated pores with a median diameter of 1102 ± 406 μm. At a percentage of weight reduction of 27% the median pore diameter could be found at 184 ± 37 μm. A percentage of weight reduction of 59% generated pores with a median diameter of 370 ± 287 μm. At a gas content of 1.6 wt% the median pore diameter was at 571 ± 354 μm. 6.3 wt% carbon dioxide in the polymer melt leaded to pores with a pore diameter of 307 ± 214 μm.

Table V shows the diameters of the connections between neighboring pores in dependence on the varied parameters. At an injection speed of 30 mm/s the pore diameter was 275 ± 89 μm. An increase in injection speed to 150 mm/s leaded to a connection size of 53 ± 27 μm. A variation in the percentage of weight reduction and the content of CO_2 produced openings with a size of 40 ± 15 μm at 27% and 59 ± 25 μm at 59% of weight reduction respectively 85 ± 45 μm at 1.6 wt% and 50 ± 19 μm at 6.3 wt% CO_2.

3.3. Mechanical properties

Fig. 6 shows the mechanical properties of the molded samples. The breaking force for the specimen processed with 25% weight reduction ($n = 20$) was 623 ± 124 N. The elongation at break could be found at 190 ± 39%. Compared to that a percentage of weight reduction of 59% ($n = 20$) leaded to a breaking force of 249 ± 105 N and an elongation at break of 76 ± 41%.

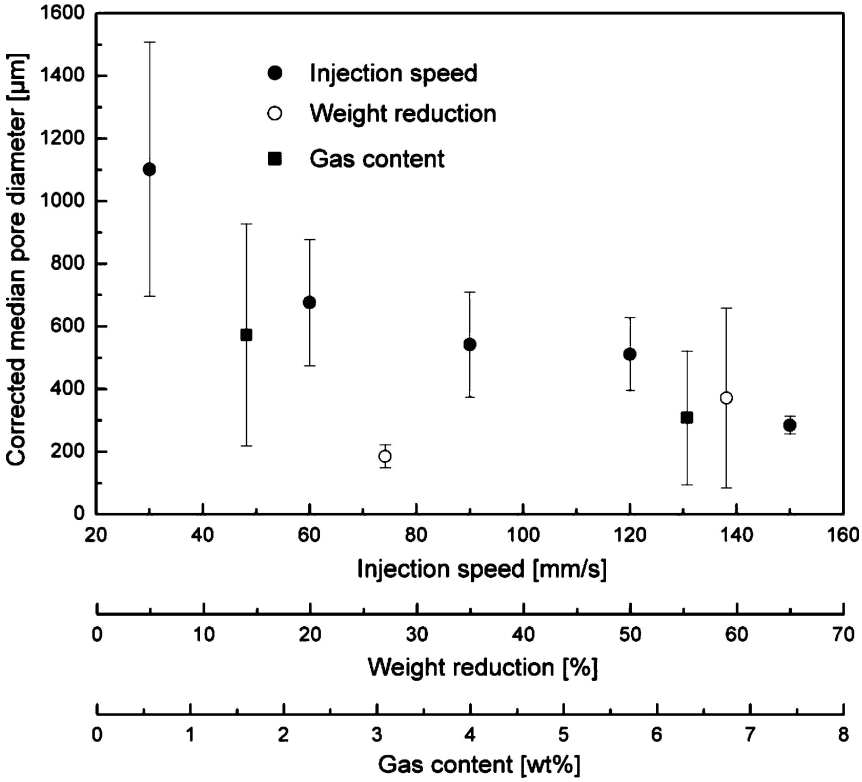

Figure 5 Corrected median pore diameter in dependence on the injection speed, the percentage of weight reduction, and the gas content.

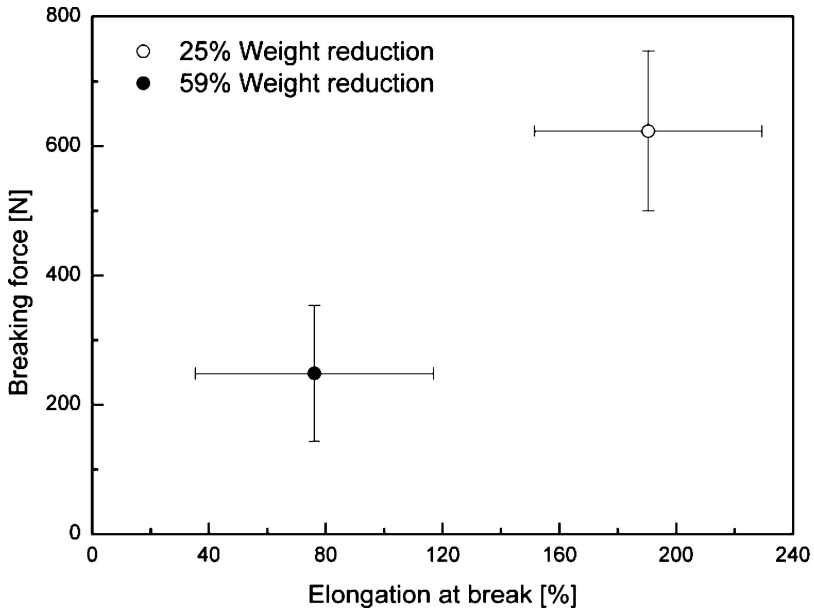

Figure 6 Mechanical properties of the samples in dependence on the percentage of weight reduction.

4. Conclusion

It was observed that the pore morphology depended on several adjustable processing parameters. The pore size and the pore size distribution were adjustable by the injection speed, the percentage of weight reduction and the content of carbon dioxide in the polymer melt. The porosity of the samples was not much influenced by these parameters. The injection speed that generates the rate of the pressure drop which is a main factor to generate nucleation sites [12, 13], had a major effect on pore size and pore size distribution. An increase in injection speed decreased the pore sizes and caused a narrower pore size distribution. When comparing the results of the pore sizes obtained from mercury intrusion porometry and image analysis it can be seen that the pores measured by porometry are much smaller than those measured by image analysis. This was likely caused by the so-called inkstand effect. This means that a small pore with a large void behind appears as many small pores in the pore size distribution curve. The result showed that an increase in injection speed from 30 to 150 mm/s decreased the corrected median pore diameter from 1102 to 284 μm. The anisotropic orientation of the pores comes about because the mechanical stresses generated during foaming are not distributed uniformly through the volume

of the polymer foam. Therefore the gas bubbles tend to expand along the directions of minimum local stress [14].

At a percentage of weight reduction of 27% the corrected median pore diameter was found to be 184 μm. A degree of weight reduction of 59% generated pores with a median diameter of 370 μm. Lower degrees of weight reduction caused structures with a narrow pore size distribution. A high degree of weight reduction leaded to a non uniform cell structure. This effect is verified by literature data [15]. At lower weight reduction the skin of the part was much thicker (results not shown) and the parts were much harder to remove from the mold. An influence of the percentage of weight reduction on the degree of interconnection was not found whereas the size of the connections at a high percentage of weight reduction was larger with a larger standard deviation. A percentage of weight reduction up to 59% was achieved. Further weight reduction was not possible since the molded part could not be removed from the mold. The percentage of weight reduction had a major effect on the mechanical properties of the porous samples. The breaking force and also the elongation at break for the specimen processed with 25% weight reduction are 2.5 times higher than those obtained at a percentage of weight reduction of 59%. Since there was no significant influence of the weight reduction on porosity this effect must result from the thicker skin of the samples processed with the lower degree of weight reduction.

At a gas content of 1.6 wt% the mean pore size diameter was at 170 μm whereas a gas content of 6.3 wt% shifted the mean pore size to 12 μm. It is known that a high gas content leads to more nucleation sites and thus smaller pores [15]. The results obtained from mercury intrusion measurements differed much from those obtained from image analysis. The samples were processed with a high percentage of weight reduction which caused a very broad pore size distribution. As image analysis only exploits a small detail of the porous structure a few large pores among many small pores will increase the median pore diameter and also leads to a huge standard deviation.

The reproducibility of the processing method concerning the porosity was proven. Overall, samples with a median porosity of 69.9 $\pm$ 3.2% ($n = 19$) were produced.

In this study it has been shown that MuCell® technology for injection molding is a useful processing method to generate porous cell carriers made of thermoplastic polyurethane in a large scale. The processed samples show an open porous structure which was achieved without the use of additives such as NaCl.

References

1. A. G. MIKOS, A. J. THORSEN, L. A. CZERWONKA, Y. BAO, R. LANGER, D. N. WINSLOW and J. P. VACANTI, *Polymer* **35** (1994) 1068.
2. D. J. MOONEY, S. PARK, P. M. KAUFMANN, K. SANO, K. MCNAMARA, J. P. VACANTI and R. LANGER, *J. Biomed. Mater. Res.* **29** (1995) 959.
3. R. C. THOMSON, M. J. YASZEMSKI and J. M. POWERS, *J. Biomater. Sci. Polym. Ed.* **7** (1995) 23.
4. H. LO, M. S. PONTICIELLO and K. W. LEONG, *Tissue. Eng.* (1995) 15.
5. K. WHANG, T. K. GOLDSTICK and K. E. HEALY, *Biomaterials* **21** (2000) 2545.
6. D. J. MOONEY, D. F. BALDWIN, N. P. SUH, J. P. VACANTI and R. LANGER, *ibid.* **17** (1996) 1417.
7. H. J. HAUGEN, in "Development of an Implant to Treat Gastro-Oesophageal Reflux Diseases" (Ph.D. Thesis, Technical University Munich, 2004).
8. H. HAUGEN, V. RIED, M. BRUNNER, J. WILL and E. WINTERMANTEL, *J. Mater. Sci. Mater. M.* **15** (2004) 343.
9. N. M. K. LAMBA, K. A. WOODHOUSE and S. L. COOPER, in "Polyurethanes in Biomedical Applications" (CRC Press, Boca Raton, 1998) p. 181.
10. H. KAWASHIMA and M. SHIMBO, *Cell. Polymers* **22** (2003) 175.
11. B. A. RODEHEAVER and J. S. COLTON, *Polym. Eng. Sci.* **41** (2001) 380.
12. C. B. PARK, D. F. BALDWIN and N. P. SUH, *ibid.* **35** (1995) 432.
13. V. GOODSHIP, R. L. STEWARD, R. HANSELL, E. O. OGUR and G. F. SMITH, *Cell. Polymers* **23** (2004) 25.
14. F. A. SHUTOV, in "Handbook of Polymeric Foams and Foam Technology" (Hanser, Munich, 1991) p. 30.
15. K. T. OKAMOTO, in "Microcellular Processing" (Carl Hanser, Munich, 2003) p. 177.

Received 10 December 2004
and accepted 7 March 2005